Gas hydrate property measurements in porous sediments with resonant ultrasound spectroscopy

B. P. McGrail,[1] S. Ahmed,[2] H. T. Schaef,[1] A. T. Owen,[1] P. F. Martin,[1] and T. Zhu[3]

Received 3 October 2005; revised 30 October 2006; accepted 20 December 2006; published 5 May 2007.

[1] Resonant ultrasound spectroscopy was used to characterize a natural geological core sample obtained from the Mallik 5L-38 gas hydrate research well at high pressure and subambient temperatures. Using deuterated methane gas to form gas hydrate in the core sample, it was discovered that resonance amplitudes are correlated with the fraction of the pore space occupied by the gas hydrate crystals. A pore water freezing model was developed that utilizes the known pore size distribution and pore water chemistry to predict gas hydrate saturation as a function of pressure and temperature. The model showed good agreement with the experimental measurements and demonstrated that pore water chemistry is the most important factor controlling equilibrium gas hydrate saturations in these sediments when gas hydrates are formed artificially in laboratory pressure vessels. With further development, the resonant ultrasound technique can provide a rapid, nondestructive, field portable means of measuring the equilibrium *P-T* properties and dissociation kinetics of gas hydrates in porous media, determining gas hydrate saturations, and may provide new insights into the nature of gas hydrate formation mechanisms in geologic materials.

Citation: McGrail, B. P., S. Ahmed, H. T. Schaef, A. T. Owen, P. F. Martin, and T. Zhu (2007), Gas hydrate property measurements in porous sediments with resonant ultrasound spectroscopy, *J. Geophys. Res.*, *112*, B05202, doi:10.1029/2005JB004084.

1. Introduction

[2] Clathrate hydrates are solid crystalline "inclusion" compounds that form when water (the host) is exposed to small hydrophobic molecules (the guest), such as methane, ethane, H_2S, and CO_2, at appropriate pressures and temperatures [*Englezos*, 1993; *Sloan*, 1998]. When the guest molecule is a constituent of natural gas, clathrate hydrates are also referred to as gas hydrates [*Sloan*, 1998].

[3] Gas hydrates occur principally in two types of geologic settings: (1) on land in permafrost regions where cold temperatures persist in shallow sediments, and (2) in sediments at water depths greater than about 500 m where high pressures dominate [*Kvenvolden et al.*, 1993]. Although estimates of the amount of in situ gas hydrate vary considerably, even a conservative estimate [*Kvenvolden*, 1995] puts the amount of gas present as gas hydrate in the earth and seas at about 10^{15} m^3 at standard temperature and pressure. The carbon mass in gas hydrate exceeds that in all conventional fossil energy reserves by as much as a factor of 2, but before large-scale commercial recovery of natural gas from gas hydrates can be attempted, important issues regarding reservoir stimulation techniques, safety, and cost must be addressed through reservoir modeling.

[4] Thermodynamic and kinetic data for gas hydrates and physicochemical properties of hydrate-bearing sediments are critically needed inputs for reservoir modeling. A large body of thermodynamic data exists for various clathrate hydrates in pure water, seawater, and other aqueous systems [*Sloan*, 1998]. However, the effects of geologic media on hydrate stability have received comparatively little attention, although most natural gas hydrates are embedded in porous rocks and sediments. Montmorillonite clay was found to promote methane hydrate formation by lowering the pressure or increasing the temperature at which gas hydrates form at the clay mineral surface [*Cha et al.*, 1988; *Vysniauskas and Bishnoi*, 1983]. Very similar marine sediments, however, were reported to act as gas hydrate formation inhibitors [*Clennell et al.*, 1999]. Significant differences in the dissociation behavior of gas hydrates synthesized in the laboratory versus naturally occurring hydrates have been reported [*McGrail et al.*, 2005]. The fundamental physics and chemistry associated with gas hydrate formation in porous media and the physicochemical properties of the gas hydrates and sediments remain poorly understood.

[5] One problem limiting data collection on gas hydrate properties in porous media is the experimental difficulty associated with the measurements. Conventional stirred pressure cells are not suitable for working with intact sediments and core samples [*Dallimore and Collett*, 1995; *Davidson et al.*, 1986]. Techniques such as the quartz crystal microbalance [*Mohammadi et al.*, 2003] are also not adaptable to use with porous media. Pressure change is the most

[1]Applied Geology and Geochemistry Department, Pacific Northwest National Laboratory, Richland, Washington, USA.
[2]Applied Physics and Materials Characterization Department, Pacific Northwest National Laboratory, Richland, Washington, USA.
[3]Petroleum Engineering Department, University of Alaska, Fairbanks, Alaska, USA.

0148-0227/07/2005JB004084$09.00

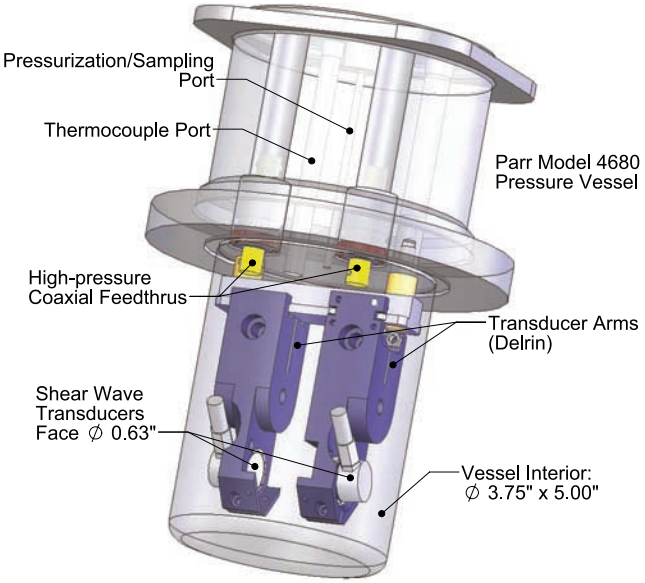

Figure 1. Schematic of resonant ultrasound spectrometer sample stage and pressure housing.

common method of monitoring gas hydrate equilibria in porous media [*Handa and Stupin*, 1992; *Uchida et al.*, 2002; *Zhang et al.*, 2003], but pressure alone does not provide information on gas hydrate saturations in the sample or other important physical properties. In addition to pressure, *Hayashi* [1999] also measured electrical resistance in pack beds of glass beads and a Berea sandstone as a means of tracking gas hydrate formation.

[6] Acoustical measurements on hydrate-bearing sediments have been performed by a number of researchers. Most of these have been done at atmospheric pressure with water-soluble hydrate formers [*Berge et al.*, 1999; *Guerin and Goldberg*, 2005; *Kunerth et al.*, 2001; *Pearson et al.*, 1986]. *Winters et al.* [1994, 2004] have performed *P* wave measurements at pressure and temperature. *P* wave velocity values were found to range from 2.4 to 2.9 km/s; velocities decreased to 1.7 to 1.8 km/s after dissociation.

[7] In this work, a new method for measuring gas hydrate properties in porous media is described that utilizes resonant ultrasound spectroscopy (RUS). Resonance methods have been performed before on gas hydrate core samples but at much lower seismic frequencies [*Priest et al.*, 2005]. The RUS method has several advantages over traditional pulsed wave ultrasound measurements. The technique is path independent, so for hydrate-bearing core samples that are nonisotropic, multiple measurements from different locations and directions are not needed. No transducer bonding on the sample surface is employed; differential thermal contraction between the specimen and transducer does not impact the measurement, and gas hydrate samples can undergo multiple freezing/thawing cycles or compression-decompression with pressure changes without concern over transducer adhesion. That is not to imply that transducer contact has no effect on the response signals. Transducer contact and drive amplitude do affect response amplitudes, and some low-amplitude resonances may not be detectable in certain contact configurations. However, given several important advantages of the method, it is surprising how few applications of RUS to examine geological materials have been reported [*Ulrich and Darling*, 2001; *Ulrich et al.*, 2002; *Zadler et al.*, 2004]. Studies at elevated pressure have been limited to fused silica [*Isaak et al.*, 1998; *Zhang et al.*, 1998]. Hence the present work represents a unique application of RUS in the examination of geologic specimens at high pressure and with the potential for phase changes occurring from the formation/dissociation of a crystalline solid (gas hydrate) in the sample pore space.

2. RUS Method

[8] Readers interested in the theory and techniques employed in RUS are referred to the review paper by *Leisure and Willis* [1997] and book by *Migliori and Sarrao* [1997]. Briefly, RUS involves sweeping a low-amplitude acoustic excitation through a range of frequencies using a driving transducer contacting a corner, edge, or face of the sample. The response signal is captured with a receiving transducer contacting an opposing surface or edge. Response signal amplitude becomes large in the vicinity of a natural vibrational mode of the sample. For homogeneous samples with simple geometry, such as parallelepipeds and cylinders, or single crystals with known symmetry, analytical formulas have been derived that can be used in conjunction with nonlinear regression methods to deduce elastic moduli [*Migliori and Sarrao*, 1997]. Interpretation of RUS spectra on polycrystalline, heterogeneous geological specimens is considerably more complex [*Ulrich et al.*, 2002; *Zadler et al.*, 2004]. Gas-phase viscous coupling with the sample surface may also impact the resonance spectra when conducting measurements at high pressure [*Beck*, 2004; *Isaak et al.*, 1998]. In the present work, our interest is in monitoring relative changes in resonance response; predicting resonance peaks and extracting quantitative mechanical property information from the spectra presented in this paper is an ongoing area of research that will be the subject of a future publication.

2.1. RUS Apparatus

[9] Experiments were conducted in a custom-designed, 1-L internal volume, fixed-head bench top model 4680 (Parr Instrument Company, Illinois), high-pressure reactor system shown in Figure 1. Two transducer supports with side-to-side movement and spring tension were mounted inside the lid suspending the sample. Modifications also include a welded cooling jacket, a 1.3-cm diameter sapphire window for viewing the sample and conducting optical spectroscopy, and high-pressure electrical feed troughs. Vessel temperature was controlled to ±1°C with a circulating water bath; sample temperature was monitored with a thermocouple that extended to within 1 cm of the sample surface.

[10] Resonance spectra were collected with a Modulus II RUS system (Dynamic Resonance Systems, Powell, WY). The unit has a digitally synthesized/filtered heterodyne swept-sine signal analyzer. All data were collected with an intermediate frequency (IF) of 977 Hz, 10 IF cycles processed for each data point, 50-ms delay per cycle, and 800 data points per spectrum. Resonance spectra were collected with either of two types of piezoelectric transducers: (1) 8-mm diameter PZT-5A ceramic longitudinal wave transducers with a transducer frequency of 1 MHz and elements that

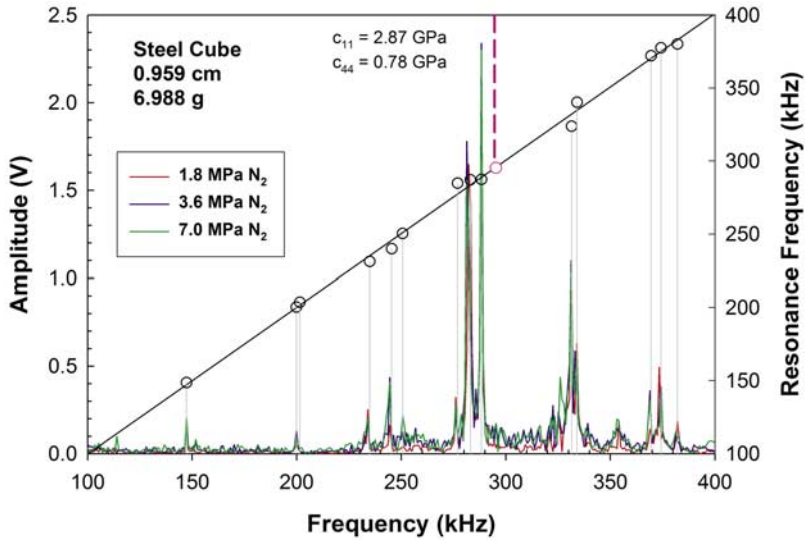

Figure 2. Resonance ultrasound spectra on steel cube standard sample as a function of N_2 pressure. Open circles represent predicted resonances for the sample using the regressed values for the elastic constants (c_{11} and c_{44}) shown. A predicted resonance peak at 294.6 kHz was not detected.

are rated up to 250 V peak-to-peak at 75 W, and (2) 13-mm diameter Panametrics, Inc. (Waltham, MA), V1561-RM broadband shear mode transducers with a transducer frequency of 1 MHz. The mounting holes in the sample stage were keyed to ensure alignment of the transducers with the polarization of the induced shear waves.

2.2. Instrument Verification

[11] Before conducting measurements with geologic samples, proper operation of our RUS instrumentation was checked by conducting measurements on a 304-L stainless steel cube machined from bar stock. The cube was 0.959 cm on edge, weighing 6.988 g. Resonance peak positions were calculated with the rectangular parallelepiped algorithm of Visscher (1991) and the best fit elastic constants determined from nonlinear regression [*Migliori and Sarrao*, 1997]. A comparison of the predicted and measured resonance peaks is given in Figure 2. The measured resonances agree closely with predicted values with the exception of a missing resonance peak at 294.6 kHz. The best-fit elastic constants are within 10% of previously reported values for 304-L stainless steel [*Ledbetter*, 1981]. No measurable impact of gas pressure in the chamber was observed on the resonance frequencies or amplitudes, other than a general increase in background noise in the spectra.

3. Samples and Materials

[12] The measurements reported in this paper were conducted with a natural gas hydrate bearing sediment obtained from the Mallik 5L-38 gas hydrate research well [*Dallimore and Collett*, 2005]. The Mallik 5L-38 core sample was taken from the overall interval 1075.4–1075.9 m with in situ pressure and temperature of approximately 10.5 MPa and 10°C, respectively. The sample consisted of unconsolidated arenite sand with a bulk density of 1.98 g/cm^3 [*Kulenkampff and Spangenberg*, 2005]. This sample was stored in liquid nitrogen (LN_2) when shipped from the well site and contained gas hydrate saturations ranging between 50 and 80% in portions of the core [*Lu et al.*, 2005]. An extensive set of physical and chemical data on Mallik 5L-38 samples can be found in the monograph of *Dallimore and Collett* [2005].

[13] The Mallik core was cut into a 2.6-cm-long × 2.4-cm-diameter cylinder. Its total volume and porosity was 11.8 cm^3 and 0.254, respectively. Reagent grade CH_4 was purchased from Air Liquid (La Porte, TX).

4. Experimental Methods

[14] RUS spectra were collected on the Mallik core sample under controlled pressure and temperature conditions while simultaneously monitoring gas hydrate saturations in the sample pore space by direct analysis of the gas phase. To distinguish between gas released from gas hydrate dissociation and the methane used for pressurization, deuterated methane (CD_4), purchased from Scott Specialty Gases (Longmont, CO), was used to produce gas hydrate in the core sample.

[15] The Mallik core sample was defrosted at room temperature and then placed in a 70°C oven and dried, checking the weight periodically until it remained constant. Then the core was saturated with deionized water (standing water on core, no more absorption observed). A weight was taken and the core dried to target 75% water saturation (S_w^o). The 75% saturated core was then placed into a 35-mL pressure vessel, with a spacer under the core, and sealed. A vacuum was then pulled on the chamber to remove residual air. The vessel was then pressurized to 6.9 MPa (1000 psig) using CD_4 gas. After pressurization, it was placed into a freezer and the temperature lowered to approximately −7.0°C. As the temperature stabilized, the pressure dropped to 5.2 MPa; the vessel was then repressurized to 6.9 MPa. Every 2 to 3 days over a 2-week period, it was cycled between a refrigerated bath at 0.0°C and the freezer. The pressure vessel was kept in the freezer at approximately −6

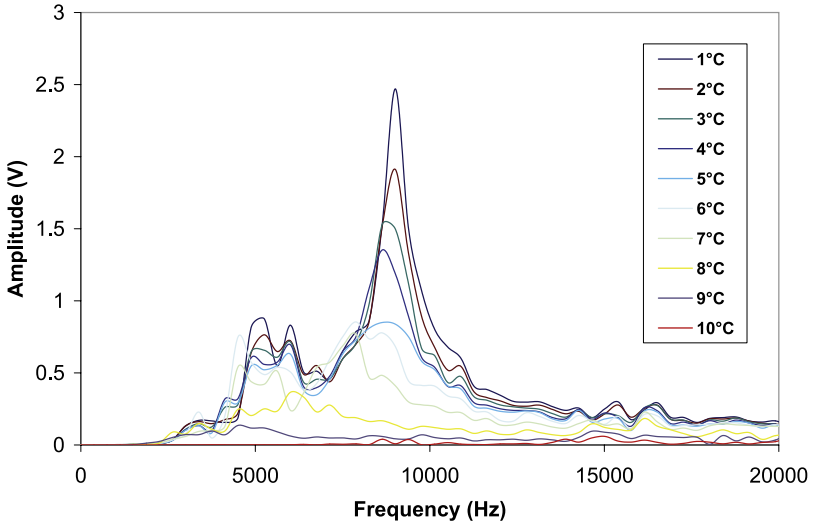

Figure 3. Shear mode resonance spectra for Mallik 5L-38 core sample containing CD_4-hydrate.

to −7°C for about 10 days prior to transferring the core sample to the RUS chamber as described below.

[16] To transfer the CD_4 soaked core into the RUS chamber with minimal loss of the CD_4-hydrate, the pressure vessel holding the core and the RUS chamber were chilled with liquid nitrogen. The cylindrical core was then removed from its pressure vessel and suspended between the two spring loaded transducers mounted to the lid of the Parr reactor. Once the core was in place, 2.0 mL of deionized water was added to the bottom of the 1.0-L chamber (to ensure the vapor phase remained water saturated without dissociating the gas hydrate). The RUS chamber was sealed and swept several times with CH_4 gas to remove residual air. The pressure was then raised to 6.3 MPa (900 psig) with CH_4 gas. The system was stabilized at −5.0°C and 7.2 MPa (1035 ± 10 psig). A gas sample was taken immediately to establish a baseline CD_4 partial pressure. The temperature was raised 1°C every 24 hours starting at −5.0°C and ending at 10°C. Resonance peak changes occurring with the Mallik core were monitored and recorded. A frequency sweep from 0 to 300 kHz and a gas sample were taken at each increment. As the amplitude changed over the course of the experiment, the amplifier gain setting was adjusted to keep the amplitude below 8 V. The gain ranged from 0.9 at the beginning of the experiment to 25 at the end.

[17] Gas samples were collected at predetermined intervals. Samples were collected in a piece of steel tubing with 5-mL internal volume connected with valves to the RUS chamber. The tube was evacuated with house vacuum prior to collecting each sample. The small gas amounts collected had no detectable impact on the RUS chamber pressure. The gas samples were then transferred to an evacuated 90-cm^3 stainless steel collection tube. The samples were analyzed on a Sanford Research Systems (Sunnyvale, CA) Residual Gas Analyzer (RGA) model 200 equipped with a Varian (Palo Alto, CA) V-70 turbo pump and an Edwards (Livermore, CA) ESDP12 scroll pump. Vacuum pressure was monitored with a Teledyne Electronic Technologies (Los Angeles, CA) 3DQ gauge. The RGA was controlled by a real-time Windows-based software package (Sanford Research Systems) that operated from a laptop computer. Each gas sample was introduced into the RGA through a needle valve, which was manually adjusted to maintain a constant pressure of 10^{-4} Torr. After the system stabilized, usually 5 min, data were collected every second for 10 min for three atomic mass units: 15 (CH_3), 16 (CH_4), and 20 (CD_4). A high purity CH_4 standard was analyzed immediately after each sample to track the performance of the RGA. Data collected at each channel were corrected for isotopic abundance using the appropriate factor (CH_3, 0.39568; CH_4, 0.44964; and CD_4, 0.44964). By averaging the corrected data from channels 20 and 15, a final partial pressure ratio of CD_4 to CH_4 was determined. Channel 16 was not used in the calculation because of the possibility of trace amounts of oxygen in the system.

5. Results

[18] Figure 3 shows the resonance response spectra of the Mallik core sample as temperature was raised at approximately constant pressure (see Table 1 for the measured values). The main feature of the spectra is rather broad resonance band centered at approximately 9 kHz at 1°C. Increasing the temperature causes a progressive decrease in resonance peak amplitude and shift in center frequency to lower values. The resonance band decreased to below detection after the temperature was increased to 10°C.

[19] The ratio of CD_4/CH_4 in the gas phase samples extracted during the experiment is provided in Table 1. The results show an increasing amount of CD_4 in the gas phase as the temperature was raised, which suggests that gas hydrate was dissociating after each step change increase in temperature. This result was initially surprising because the equilibrium temperature for methane hydrate in pure water at 7.5 MPa pressure is approximately 10.7°C [*Sloan*, 1998], indicating that methane hydrate should have been stable over the entire pressure-temperature range covered in this experiment. Isotope exchange would produce a trend in the gas phase data that would appear like gas hydrate dissociation, but we eliminated this possibility by holding the temperature at 8°C for an additional 3 days and sampling the gas phase each day. Because the results were all within experimental error, the isotope exchange rate was deter-

Table 1. Measured and Calculated Values of Gas Hydrate Saturation in Validation Experiment with CD_4 Hydrate in a Mallik 5L-38 Core Sample

P, MPa	T, °C	CD_4/CH_4, $\times 10^4$	S_h	S_h Model	RUS, Hz	RUS, V	RUS S_h
7.25	−5.0	2.00	0.796	0.721	–	–	–
7.26	−4.1	2.78	0.783	0.719	9011	3.21	0.783
7.29	−3.0	3.24	0.776	0.716	9011	2.89	0.756
7.31	−2.0	4.32	0.758	0.714	9011	3.00	0.766
7.34	−1.0	4.41	0.756	0.712	9011	3.01	0.766
7.36	0.0	5.62	0.737	0.708	9011	2.95	0.762
7.39	1.0	6.33	0.725	0.704	9011	2.47	0.718
7.41	2.0	8.66	0.687	0.699	9011	2.32	0.703
7.44	3.2	12.6	0.622	0.692	8636	1.53	0.612
7.46	4.0	13.7	0.604	0.685	8636	1.35	0.587
7.48	4.9	12.9	0.618	0.675	8636	0.85	0.503
7.51	5.9	16.1	0.566	0.661	7885	0.85	0.504
7.54	6.9	19.9	0.503	0.639	7885	0.77	0.487
7.56	8.0	18.6	0.525	0.598	6008	0.37	0.380
7.59	9.0	22.6	0.460	0.517	4506	0.14	0.273
7.61	10.0	45.5	0.085	0.248	3755	0.00	0.059
7.61	10.0	50.2	0.008	0.248	–	–	–
7.64	11.0	50.4	0.005	0.000	bd[a]	bd	–
7.66	11.9	51.4	−0.012	0.000	bd	bd	–
7.69	13.0	50.8	−0.001	0.000	bd	bd	–

[a]bd = peak amplitude below detection.

mined to be much smaller than the changes occurring from each step increase in temperature. Methane hydrate was clearly dissociating in core sample pore space, although the *P-T* conditions were well within the bulk equilibrium stability field.

6. Discussion

6.1. Methane Hydrate Saturation

[20] The seemingly unusual stability behavior of methane hydrate in the Mallik core sample detected by RUS and gas phase analysis requires further explanation. As we will show quantitatively, dissociation can be related to the effect of salts in the pore fluid. We first need to calculate the methane hydrate saturation in the core sample from the ratio of CD_4/CH_4 determined from the gas sample analysis (Table 1). The maximum possible ratio of CD_4/CH_4 (n^o_{DH}) in the RUS vessel can be calculated assuming complete conversion of the water in the core sample to CD_4 hydrate. The number of possible moles of CD_4 stored as gas hydrate in the core was calculated from the known mass of water added to the core and assuming a hydration number of 6 for the CD_4 hydrate. The number of moles of CH_4 in the RUS chamber was computed from the gas law using the measured equilibrium pressure at the start of the experiment (7.3 MPa), temperature (−5°C), internal volume of the chamber less volume occupied by the core, transducer stage, etc. (809 cm^3), and using a compressibility factor of 0.82 for CH_4 [*Lemmon et al.*, 2005]. The maximum amount of CH_4 that could be consumed from hydrate formation with the 2 mL of water added in the bottom of the chamber amounted to less than 0.6% of the total CH_4 in the vessel and so was considered negligible. The calculated value is $n^o_{DH} = 0.0056$, which can be compared with the measured value at the end of the experiment of $\bar{n}_{DH} = 0.0051$ obtained by averaging the last four data points. Hence about 91% of the available water was actually converted to CD_4 hydrate, giving a starting gas hydrate saturation in the core of $S^o_h = 0.91 \times S^o_w \times (\rho^o_w/\rho^o_h) = 0.91 \times 0.75 \times (1.01/0.79) = 0.86$, where ρ^o_w is the initial density of the pore fluid phase, and ρ^o_h is the density of the S-I empty gas hydrate crystal lattice. Using the measured values of n_{DH} for each temperature, S_h was then calculated from

$$S_h = \frac{S^o_w(\bar{n}_{DH} - n_{DH})\rho^o_w}{n^o_{DH}\rho^o_h} \quad (1)$$

and these values are reported in Table 1. The pore fluid density is actually a function of temperature and pressure, but these changes are relatively small over the range of our test conditions and so were neglected.

[21] As was mentioned in section 1, many studies have been performed examining the impact of porous media and pore size on gas hydrate equilibrium *P-T* properties [*Anderson et al.*, 2003; *Clennell et al.*, 1999; *Henry et al.*, 1999; *Klauda and Sandler*, 2001; *Kuhs et al.*, 2000; *Uchida et al.*, 2002; *Wilder et al.*, 2001; *Zatsepina and Buffett*, 2001]. To help interpret the data regarding gas hydrate stability in these samples, in the next section, we develop a new model designed for computation of equilibrium gas hydrate saturation moderated by the impact of pore size and including the impact of salts.

6.2. Pore Water Freezing Model

[22] Consider a spherical pore of radius r initially containing only vapor and liquid phases. After a step change in temperature to a new value T below the bulk equilibrium temperature T_m, water ice and/or gas hydrate forms in the pore space reducing the radius to a new value r_p. If the initial salt concentration in the pore is C_o, the new salt concentration in the residual pore water is given by

$$C_p = C_o \frac{r^3}{r_p^3}. \quad (2)$$

The reduced pore size now has a higher radius of curvature compared with the initial pore. There are a number of ways to model the effect of curvature of the hydrate-aqueous phase interface on the equilibrium properties of water ice and gas hydrates [*Christoffersen and Tulaczyk*, 2003; *Klauda and Sandler*, 2001]. We have elected to use the model of *Jiang et al.* [2001] where the minimum pore size that can contain ice/or gas hydrate is given by

$$r_p = r_c[1 + (1 - \alpha)/\ln(T/T_m)] \quad (3)$$

where r_c is the critical radius for an ice or gas hydrate crystal, and α is a mean square displacement ratio for atoms of the surface versus atoms in the bulk crystal ($\alpha = 1.66$ for ice nanocrystals). The ice equilibrium or gas hydrate equilibrium temperature is computed from any convenient equation of state (EOS) program as represented by the nonlinear function

$$T_m = f(C_p, P_l) \quad (4)$$

where P_l is the equilibrium pressure of the liquid phase in a pore given by [*Klauda and Sandler*, 2001]:

$$P_l = P_g - \frac{2\sigma_{hl}}{r_p} \quad (5)$$

where P_g is the gas pressure and σ_{hl} is the interfacial tension between the hydrate and liquid phases, assumed to be 27 mJ/m^2. Equations (2)–(4) represent a nonlinear system of three equations that can be solved for the three unknowns T_m, C_p, and r_p as a function of r. Thus the volume fraction of a pore containing ice or gas hydrate at equilibrium is given by

$$V_f(r) = 1 - \left(\frac{r_p(r)}{r}\right)^3. \quad (6)$$

The total initial pore volume is given by

$$V_p^o = N_p \int_0^\infty p(r) V_p(r) dr \quad (7)$$

where N_p is the number of pores in the sample, $p(r)$ is the pore size probability distribution function for the porous medium, and $V_p(r) = 4/3\pi r^3$. The volume of water filling the pore space is then given by an analogous expression

$$V_w = N_p \int_0^z p(r) V_p(r) dr \quad (8)$$

where z is the largest pore radius in the sample containing water; this allows the larger pores in the sample to drain first (as a consequence of capillary suction) to accommodate situations where the pore space is not fully water saturated. Hence the volumetric water saturation is

$$S_w^o = \frac{V_w}{V_p^o} = \frac{\int_0^z p(r) V_p(r) dr}{\int_0^\infty p(r) V_p(r) dr} \quad (9)$$

Equation (9) can be solved for z, assuming S_w^o is known or measured in a sample. Assuming the pore size distribution is known for the sample, the ice or gas hydrate saturation (S_h) at equilibrium can then be computed from

$$S_h = \frac{\int_{r_m}^z p(r) V_p(r) V_f(r) dr}{\int_0^\infty p(r) V_p(r) dr} \quad (10)$$

where r_m is the minimum pore radius below which no ice or gas hydrate can form. The value of r_m is computed by setting $C_p = C_o$ and solving equation (3).

$$r_m = r_c[1 + (1 - \alpha)/\ln(T/f(C_o, P_l))] \quad (11)$$

The value of S_h computed with equation (10) is the maximum gas hydrate saturation; no limitations on the amount of the guest available are taken into account (this is a trivial additional constraint to add into the model).

6.3. Comparison With Pore Water Freezing Model

[23] Having computed the gas hydrate saturations in the core as temperature was changed during the experiment, these values can be compared with predicted values based on the pore water freezing model discussed in section 6.2. To do so, the pore size distribution and pore fluid chemistry in the sample must be known. Pore size distribution for sandy sequences at the Mallik site have been measured by *Katsube et al.* [1999]. Sandy samples similar to the sample used in this study show an essentially unimodal pore size distribution, with the exception of <2% very fine pore size material around 6–7 nm. We fit the data reported by *Katsube et al.* [1999] for his EJA-6 sand sediment sample to a Gaussian distribution

$$p(r) = a_1 \exp\left[-\frac{1}{2}\left(\frac{r - r_1}{b_1}\right)^2\right] \quad (12)$$

where a_1, b_1, and r_1 are regression coefficients. The fit parameters are $a_1 = 0.22\ \mu m^{-1}$, $b_1 = 7.81\ \mu m$, and $r_1 = 24.0\ \mu m$ with an $R^2 = 0.98$. Pore water geochemistry studies also have been done for Mallik core samples. For the depth interval of the Mallik 5L-38 sample used in this study, averaging the data of *Matsumoto et al.* [2005] gives an Na pore water concentration of 230 mM, which is considerably freshened from seawater at 468 mM, an indicator that gas hydrate was present in the sample in situ. We also measured the salt content in a few of our samples and found values within approximately 30% of those reported by *Matsumoto et al.* [2005]. We elected to use the data of Matsumoto et al. for the calculations in this study.

[24] The parameters r_c, α, and T_m for methane hydrate are needed to solve equation (3) for r_p and equation (11) for r_m. We use the relationship $r_c = 3h$ of *Jiang et al.* [2001] to compute r_c, where $h = 1.2$ nm, the unit cell dimension of the sI gas hydrate [*Sloan*, 1998]. The parameter α is given by [*Jiang et al.*, 2001]

$$\alpha = \frac{\Delta S_d}{3R} + 1 \quad (13)$$

where ΔS_d is the entropy of melting of the bulk crystal and R is the gas constant. Noting that $\Delta S_d = \Delta H_d/T$ where ΔH_d

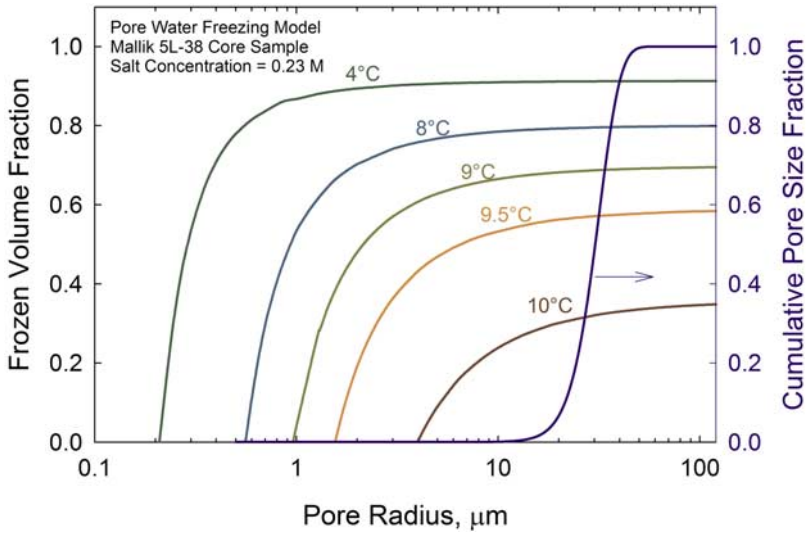

Figure 4. Calculated fraction of pore volume containing gas hydrate in Mallik 5L-38 core sample as a function of temperature and initial pore size. Pressure at each temperature is given in Table 1.

is the enthalpy of dissociation, and using the correlation [*Holder et al.*, 1988]

$$\Delta H_d = 4.18(13500 - 4T) \quad (14)$$

temperature-dependent values of α were calculated ranging from 2.29 at −5°C to 2.15 at 10°C.

[25] At large degrees of subcooling from the bulk gas hydrate dissociation temperature, salt exclusion from the gas hydrate crystals can generate quite high salt concentrations in the residual pore water. Hence accurately calculating the effect of high salt concentrations on the bulk equilibrium properties is required. Initial calculations of bulk methane hydrate equilibrium properties were done using UAFHYD, an equation of state (EOS) simulator developed at the University of Alaska [*Zhu et al.*, 2005]. The UAFHYD module utilizes Pitzer equations to correct the activity coefficient of water at high ionic strength. However, essentially identical results were obtained using the correlation developed by *Ostergaard et al.* [2005], which gives good accuracy up to 26.5 mass% (6.2 M) NaCl. Because this model is much simpler to implement computationally, we elected to use it to compute bulk methane hydrate equilibrium properties as a function of pressure, temperature, and concentration of NaCl.

[26] Using the starting water saturation in the core sample of 0.75, equation (9) was solved giving z = 35.1 μm. For each *P-T* condition of the experiment, equations (3)–(5) were then solved simultaneously in Mathematica (registered trademark of Wolfram Research) and values of V_f generated over a wide range of pore sizes. Selected results are shown in Figure 4 and compared with the cumulative pore size distribution function for the core sample. The results show that even very small degrees of cooling below the equilibrium temperature produce gas hydrate in pores below 10-μm diameter. In comparing the pore size distribution of the Mallik sediment with the calculated V_f values, one can immediately see that at temperatures <9°C in these experiments, the V_f values are nearly constant over the range of pore sizes prevalent in the sediment. Hence the pore size distribution itself has little impact on the equilibrium gas hydrate saturations. It is also important to point out that the freezing profiles illustrated in Figure 4 occur over a range of mesopores between 100 and 0.1 μm that are not significantly impacted by Gibbs-Thomson effects related to pore radius. Instead, the gas hydrate saturations are controlled by the salt concentrations in the residual pore water. As was stated previously, quite high salt concentrations are calculated in the residual pore water, reaching over 3 M at temperatures below 1°C and 5.7 M at −5°C. Hence in the absence of mass transport effects to moderate salt concentrations, pore water chemistry is the most important control on gas hydrate saturations produced in these sediments under laboratory conditions. The important aspect of the pore freezing model is that it illustrates how a unique equilibrium point associated with bulk methane hydrate does not apply in porous media, being replaced by a continuous function dependent upon pore fluid chemistry and a statistical distribution of pore sizes that is itself a function of the degree of subcooling below the bulk equilibrium temperature.

[27] Using the calculated freezing profile data as illustrated in Figure 4, equation (10) was solved to compute gas hydrate saturations for each *P-T* condition given in Table 1. The resulting S_h values are reported in Table 1 and also shown in Figure 5. The calculated values show good agreement with the experimental data, but S_h values are slightly underpredicted at temperatures below −2°C. This may be due to the simplified geometrical treatment of the pore geometry. Another important assumption in the model is that gas hydrate formation occurs uniformly in the sense that gas hydrate fills the pores to the extent physically possible following the original pore size distribution in the sample. However, gas hydrate growth in porous media is known to be quite heterogenous [*Gupta et al.*, 2006]. Finally, although NaCl is by far the most concentrated component in Mallik sediment pore water, our analysis has neglected the effects of the other cations present that

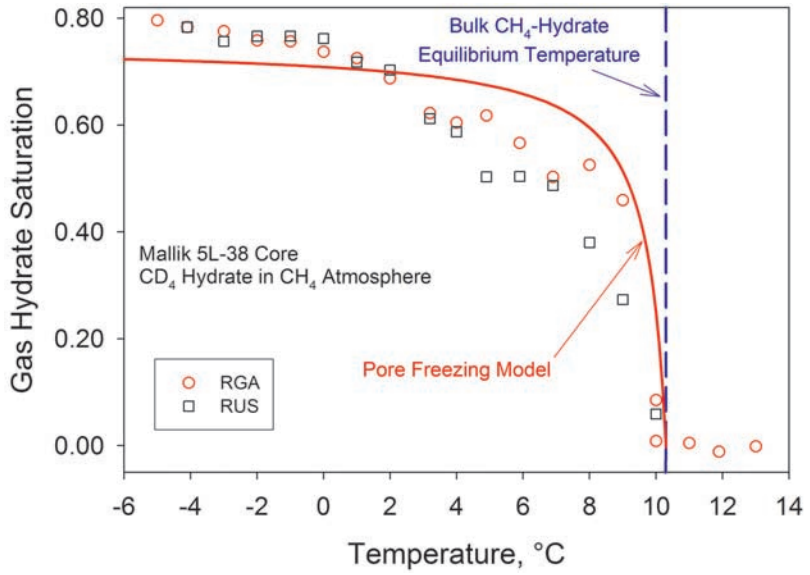

Figure 5. Comparison of gas hydrate saturations as determined from direct gas phase analysis of CD_4 concentration versus peak amplitude from RUS measurements. Red lines were calculated using the pore water freezing model discussed in section 6.3.

include millimolar level concentrations of Ca and Mg among several cations and anions.

6.4. RUS Data Analysis

[28] Resonance peak frequency and amplitude for the principal resonance peak shown in Figure 3 are given in Table 1. At the present time, we do not have a first-principles model available that would allow computation of the effect of pressure, temperature, and gas hydrate saturation on resonance response. To explore potential correlations between resonance peak amplitude and gas hydrate saturations, we calculated S_h values from the amplitude values given in Table 1 assuming a linear, square root, and cube root dependence of the amplitudes on S_h. The best correlation with the measured S_h values is obtained using the cube root dependence, and these data are plotted in Figure 5. The correlation with the measured data is excellent, but a quantitative theory is needed to explain the mechanism for the observed power law dependence.

[29] The classical approach to analyzing RUS spectra is based on the variational method of solving the free-body resonance problem [*Migliori and Sarrao*, 1997], which requires the solution of the eigenvalue problem

$$\left(\overline{\overline{\Gamma}} - \omega^2\,\overline{\overline{E}}\right)\vec{a} = \vec{0}. \tag{15}$$

[30] The elements of the matrices $\overline{\overline{\Gamma}}$ and $\overline{\overline{E}}$ are given by

$$\begin{aligned} E_{\lambda\alpha\lambda'\alpha'} &= \delta_{\alpha\alpha'} \int_{V_c} \Phi_\lambda \rho \Phi_{\lambda'} \mathrm{d}v \text{ and } \Gamma_{\alpha\lambda\alpha'\lambda'} \\ &= \int_{V_c} \Phi_{\lambda,\beta} c_{\alpha\beta\alpha'\beta'}(\vec{r}) \Phi_{\lambda',\beta'} \mathrm{d}v. \end{aligned} \tag{16}$$

[31] In the foregoing equation, $\Phi_\lambda = x^l y^m z^n$, where $\lambda = (l, m, n)$ is a triplet of three nonnegative integers, ρ and c_{ijkl} are the density and the elastic constants, respectively, of the sample, and V_c is the volume of the free body. On a truncated set Ω such that $l + m + n \leq N$, the displacement vector is written as

$$u_i = \sum_{\lambda\in\Omega} a_{i\lambda}\Phi_\lambda, \qquad i = 1, 2, 3. \tag{17}$$

The form of the integrals appearing in the elements of $\overline{\overline{\Gamma}}$ and $\overline{\overline{E}}$ is $\int_{V_c} x^p y^q z^r \mathrm{d}v$. For a right circular cylinder having a base radius d and height l [*Visscher et al.*, 1991],

$$\begin{aligned} \int_{V_c} x^p y^q z^r \mathrm{d}v &= 4\pi \left(\frac{d}{2}\right)^{p+q+2} \left(\frac{l}{2}\right)^{r+1} \frac{(p-1)!!(q-1)!!}{(r+1)(p+q+2)!!}, \quad \forall \quad \text{even } p, q, r \\ &= 0 \quad \text{otherwise} \end{aligned} \tag{18}$$

The eigenvalues of equation (17) are the resonant frequencies, and the eigenvectors $\vec{a}$ are the coefficients of the actual displacement functions in terms of the basis functions. These coefficients can be used to describe the two-dimensional pattern of the oscillating object surface, which is a signature of the individual mode of vibration.

[32] The preceding analysis is quite useful in correlating resonance frequencies with mechanical properties and vibrational modes, but it does not directly assist in developing amplitude correlations with changes in the mechanical or pore filling properties of a sample undergoing resonance oscillations. Computing normal mode amplitudes is important because they can be employed in a formulation to eliminate noise due to acoustic scattering, and address quantitatively the impact of pore filling gas hydrate on resonance modes. Unfortunately, the desired amplitude correlations cannot be developed from the solution of an eigenmode problem in a straightforward manner; the elastic wave equation must be solved directly, which is a much more computationally intensive task.

[33] Although our research group is presently engaged in development of a full solution to the elastic wave resonance

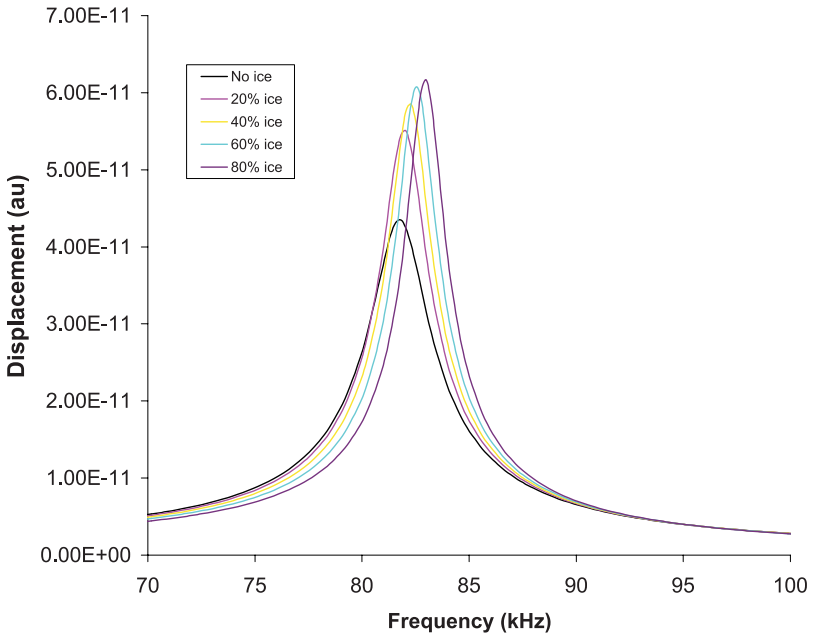

Figure 6. Computed effect of ice/hydrate volume on displacement field at the center of a cylinder face due to a point sinusoidal force at the center of the other face.

problem, a semiquantitative analysis is still possible by considering resonance phenomenon as a complex superposition of elastic waves at frequencies where the wavelengths λ are much larger than the pore sizes. To account for the presence of gas hydrate in pores, we have employed the following "linear spring in series" model for the elastic moduli

$$\frac{1}{K_{\mathrm{mix}}} = \frac{1}{(1-\nu_{\mathrm{h}})/K_{\mathrm{w}} + \nu_{\mathrm{h}}/K_{\mathrm{h}}} \tag{19}$$

where K_{mix} is the equivalent modulus of the mixture of ice/hydrate and water, K_{w} and K_{h} are the bulk moduli for water and gas hydrate, respectively, and ν_{h} is the volume fraction of gas hydrate in a pore. The bulk and the shear moduli are related to c_{IJ}, in reduced notation, through $K = c_{12} + 2c_{44}/3$, $\mu = c_{44}$. Anelasticity of real objects is introduced in the mathematical description of the resonance phenomena through the use of complex elastic constants c_{ijkl} in equation (15). The imaginary part of c_{ijkl} is related to the energy dissipation or the quality factor Q of each resonance. Introduction of complex elastic constants results in complex resonance frequencies, $\upsilon = \omega + i\gamma$, $\gamma > 0$ representing the normal mode's decay rate. Energy dissipation in isotropic solids can be described by two different Q values: bulk and shear quality factors Q_{K} and Q_{S}, respectively. Although, strictly speaking, $Q = Q(\omega)$, over a limited frequency band, Q can be assumed to be constant. With this assumption, the imaginary parts of the complex bulk and shear moduli are K/Q_{K} and μ/Q_{S}, respectively.

[34] The volume fraction of ice/hydrate present in a porous medium influences Q_{K} and Q_{S} in a complex way. It is hypothesized that the increase in the imaginary part of the complex elastic moduli due to the presence of water (damping medium) is directly proportional to the mean water-path length in the pores. Specifically, we hypothesize that $\Delta(\mathrm{Im}[K]) = \varepsilon d(1 - \nu_{\mathrm{h}}^{1/3})C_1$ and $\Delta\ (\mathrm{Im}[\mu]) = \varepsilon d(1 - \nu_{\mathrm{h}}^{1/3})C_2$, where C_1 and C_2 are model parameters. We have arbitrarily used $C_1 = 0.004$ and $C_2 = 0.003$ to compute the complex eigenvalues and eigenvectors using representative Berea sandstone properties [*Zhang et al.*, 2003]. The displacement response $\vec{s}$ at $\vec{r}$ due to a sinusoidal point force $[\vec{f}(\vec{r},t) = \vec{f}_0\ \delta(\vec{r} - \vec{r}_s)e^{i\omega t}]$ with a given polarization applied at $\vec{r}_{\mathrm{s}}$ is then computed from [*Migliori and Sarrao*, 1997]

$$\vec{s}(\vec{r}) = \sum_{i=1}^{M} \frac{v^{(i)}(\vec{r}_{\mathrm{s}}) \cdot \vec{f}_0 v^{(i)}(\vec{r})}{\omega^2 - \omega_i^2} \tag{20}$$

where $v^{(i)}(\vec{r})$, $i = 1,2,\ldots$, are the displacement eigenvectors at location $\vec{r}$ computed from equations (15) and (17), ω_i are the resonance frequencies, and $\vec{f}_0$ is a constant force vector.

[35] Figure 6 shows the computed displacement amplitude of a dominant longitudinal mode. The result clearly shows that as the volume of ice/hydrate increases, the amplitude as well as the resonance frequency increases. This is consistent with our RUS measurements and expectation that increased stiffness due to ice/hydrate formation and decreased mean water path in pores results in less attenuation of the longitudinal mode of vibration, increasing the resonance amplitude and frequency. Interestingly, the predicted attenuation behavior of vibrational modes at ultrasonic resonance frequencies is opposite that predicted from in situ seismic wave scattering [*Guerin and Goldberg*, 2005]. However, *Waite et al.* [2004] and *Kulenkampff and Spangenberg* [2005] also have observed a correlation between *P* and *S* wave amplitude and gas hydrate saturation in a Mallik core samples, which independently confirms both our new RUS measurements and theoretical interpretation thereof.

7. Conclusion

[36] In the present work, resonant ultrasound spectra were collected on a natural geological core sample at high pressure

and subambient temperatures such that methane hydrate formed in the pore space. It was discovered that resonance amplitudes are correlated qualitatively to the fraction of the pore space occupied by the gas hydrate crystals. With further experimental and theoretical development, the technique could provide a new means of detecting the presence of gas hydrate, determining gas hydrate saturations, and measuring the equilibrium *P-T* properties and dissociation kinetics of gas hydrates in porous media. A simple pore water freezing model was developed and quantitatively compared with the experimental measurements of gas hydrate saturation in the core sample. The model showed good correlation with the laboratory measurements and demonstrated that pore water chemistry is the most important factor controlling laboratory-grown gas hydrate saturations in sediments from the Mallik research well.

[37] **Acknowledgments.** The authors gratefully acknowledge the helpful comments received from several anonymous reviewers and especially Dr. William Waite. This work was supported by the US Department of Energy, Office of Fossil Energy through the National Energy Technology Laboratory, Morgantown, West Virginia, and through the Arctic Energy Office, Fairbanks, Alaska. Initial instrumentation development and reduction to practice was supported through the Laboratory Directed Research and Development Program at the Pacific Northwest National Laboratory, a multiprogram national laboratory operated by Battelle for the US Department of Energy under Contract DE-AC06-76RL01830.

References

Anderson, R., M. Llamedo, B. Tohidi, and R. W. Burgass (2003), Experimental measurement of methane and carbon dioxide clathrate hydrate equilibria in mesoporous silica, *J. Phys. Chem. B*, *107*, 3507–3514.

Beck, D. E. (2004), Rayleigh-Ritz calculation of the resonant modes of a solid parallelepiped in a pressurizing fluid, *J. Acoust. Soc. Am.*, *115*, 556–566.

Berge, L. I., K. A. Jacobsen, and A. Solstad (1999), Measured acoustic wave velocities of R11 (CCl_3F) hydrate samples with and without sand as a function of hydrate concentration, *J. Geophys. Res.*, *104*, 15,415–15,424.

Cha, S. B., H. Ouar, T. R. Wildeman, and E. D. Sloan (1988), A 3rd-surface effect on hydrate formation, *J. Phys. Chem.*, *92*, 6492–6494.

Christoffersen, P., and S. Tulaczyk (2003), Response of subglacial sediments to basal freeze-on: 1. Theory and comparison to observations from beneath the West Antarctic ice sheet, *J. Geophys. Res.*, *108*(B4), 2222, doi:10.1029/2002JB001935.

Clennell, M. B., M. Hovland, J. S. Booth, P. Henry, and W. J. Winters (1999), Formation of natural gas hydrates in marine sediments 1. Conceptual model of gas hydrate growth conditioned by host sediment properties, *J. Geophys. Res.*, *104*, 22,985–23,003.

Dallimore, S. R., and T. S. Collett (1995), Intrapermafrost gas hydrates from a deep core-hole in the Mackenzie Delta, Northwest-Territories, Canada, *Geology*, *23*, 527–530.

Dallimore, S. R., and T. S. Collett (2005), Summary and Implications of the Mallik 2002 Gas Hydrate Production Research Well Program, in *Scientific Results from the Mallik 2002 Gas Hydrate Production Research Well Program, Mackenzie Delta, Northwest Territories, Canada*, edited by S. R. Dallimore and T. S. Collett, Geological Survey of Canada, Vancouver, British Columbia.

Davidson, D. W., S. K. Garg, S. R. Gough, Y. P. Handa, C. I. Ratcliffe, J. A. Ripmeester, J. S. Tse, and W. F. Lawson (1986), Laboratory analysis of a naturally-occurring gas hydrate from sediment of the Gulf of Mexico, *Geochim. Cosmochim. Acta*, *50*, 619–623.

Englezos, P. (1993), Clathrate hydrates, *Ind. Eng. Chem. Res.*, *32*, 1251–1274.

Guerin, G., and D. Goldberg (2005), Modeling of acoustic wave dissipation in gas hydrate-bearing sediments, *Geochem. Geophys. Geosyst.*, *6*, QO7010, doi:10.1029/2005GC000918.

Gupta, A., T. J. Kneafsey, G. J. Moridis, Y. Seol, M. B. Kowalsky, and E. D. Sloan (2006), Composite thermal conductivity in a large heterogeneous porous methane hydrate sample, *J. Phys. Chem. B*, *110*, 16,384–16,392.

Handa, Y. P., and D. Stupin (1992), Thermodynamic properties and dissociation characteristics of methane and propane hydrates in 70-angstrom-radius silica-gel pores, *J. Phys. Chem.*, *96*, 8599–8603.

Hayashi, Y. (1999), Methane hydrate formation in porous media—Observation in heterogeneous model experimental systems, *J. Jpn. Pet. Inst.*, *42*, 22–29.

Henry, P., M. Thomas, and M. B. Clennell (1999), Formation of natural gas hydrates in marine sediments 2. Thermodynamic calculations of stability conditions in porous sediments, *J. Geophys. Res.*, *104*, 23,005–23,022.

Holder, G. D., S. P. Zetts, and N. Pradhan (1988), Phase-behavior in systems containing clathrate hydrates—A review, *Rev. Chem. Eng.*, *5*, 1–70.

Isaak, D. G., J. D. Carnes, O. L. Anderson, and H. Oda (1998), Elasticity of fused silica spheres under pressure using resonant ultrasound spectroscopy, *J. Acoust. Soc. Am.*, *104*, 2200–2206.

Jiang, Q., L. H. Liang, and M. Zhao (2001), Modelling of the melting temperature of nano-ice in MCM-41 pores, *J. Phys. Condens. Matter*, *13*, L397–L401.

Katsube, T. J., S. R. Dallimore, T. Uchida, K. A. Jenner, T. S. Collett, and S. Connell (1999), Petrophysical Environment of Sediments Hosting Gas Hydrate, JAPEX/JNOC/GSC Mallik 2L-38 Gas Hydrate Research Well, in *Scientific Results from JAPEX/JNOC/GSC Mallik 2L-38 Gas Hydrate Research Well, Mackenzie Delta, Northwest Territories, Canada*, edited by S. R. Dallimore, et al., pp. 109–123, Geological Survey of Canada, Vancouver, British Columbia.

Klauda, J. B., and S. I. Sandler (2001), Modeling gas hydrate phase equilibria in laboratory and natural porous media, *Ind. Eng. Chem. Res.*, *40*, 4197–4208.

Kuhs, W. F., A. Klapproth, F. Gotthardt, K. Techmer, and T. Heinrichs (2000), The formation of meso- and macroporous gas hydrates, *Geophys. Res. Lett.*, *27*, 2929–2932.

Kulenkampff, J., and E. Spangenberg (2005), Physical Properties of Cores From the JAPEX/JNOC/GSC et al. Mallik 5L-38 Gas Hydrate Production Research Well Under Simulated In Situ Conditions Using the Field Laboratory Experimental Core Analysis System (FLECAS), in *Scientific Results from Mallik 2002 Gas Hydrate Production Research Well Program, Mackenzie Delta, Northwest Territories, Canada*, edited by S. R. Dallimore and T. S. Collett, Geological Survey of Canada, Vancouver, British Columbia.

Kunerth, D. C., D. M. Weinberg, J. W. Rector, C. L. Scott, and J. T. Johnson (2001), Acoustic laboratory measurements during the formation of a THF-hydrate in unconsolidated porous media, *J. Seism. Explor.*, *9*, 337–354.

Kvenvolden, K. A. (1995), Natural-gas hydrate occurrence and issues, *Sea Technol.*, *36*, 69–74.

Kvenvolden, K. A., G. D. Ginsburg, and V. A. Soloviev (1993), Worldwide distribution of subaquatic gas hydrates, *Geo Mar. Lett.*, *13*, 32–40.

Ledbetter, H. M. (1981), Stainless-steel elastic constants at low temperature, *J. Appl. Phys.*, *52*, 1587–1589.

Leisure, R. G., and F. A. Willis (1997), Resonant ultrasound spectroscopy, *J. Phys. Condens. Matter*, *9*, 6001–6029.

Lemmon, E. W., M. O. McLinden, and D. G. Friend (2005), Thermophysical Properties of Fluid Systems, in *NIST Chemistry WebBook*, edited by P. J. Linstrom and W. G. Mallard, National Institute of Standards and Technology, Gaithersburg, MD.

Lu, H., R. Dutrisac, J. Ripmeester, F. Wright, and T. Uchida (2005), Measurements of Gas Hydrate Saturation in Sediment Cores Recovered from the JAPEX/JNOC/GSC et al. Mallik 5L-38 Gas Hydrate Production Research Well, in *Scientific Results from Mallik 2002 Gas Hydrate Production Research Well Program, Mackenzie Delta, Northwest Territories, Canada*, edited by S. R. Dallimore and T. S. Collett, Geological Survey of Canada, Vancouver, British Columbia.

Matsumoto, R., H. Tomaru, Y. F. Chen, H. Lu, and I. D. Clark (2005), Geochemistry of the Interstitial Waters of the JAPEX/JNOC/GSC et al. Mallik 5L-38 Gas Hydrate Production Research Well, in *Scientific Results from Mallik 2002 Gas Hydrate Production Research Well Program, Mackenzie Delta, Northwest Territories, Canada*, edited by S. R. Dallimore and T.S. Collett, Geological Survey of Canada, Vancouver, British Columbia.

McGrail, B. P., J. S. Young, P. F. Martin, and M. L. Alexander (2005), Characterization of Mallik 5L-38 Core Samples in the Environmental Scanning Electron Microscope, in *Scientific Results from Mallik 2002 Gas Hydrate Production Research Well Program, Mackenzie Delta, Northwest Territories, Canada*, edited by S. R. Dallimore and T.S. Collett, Geological Survey of Canada, Vancouver, British Columbia.

Migliori, A., and J. L. Sarrao (1997), *Resonant Ultrasound Spectroscopy*, 201 pp. John Wiley, Hoboken, N. J.

Mohammadi, A. H., B. Tohidi, and R. W. Burgass (2003), Equilibrium data and thermodynamic modeling of nitrogen, oxygen, and air clathrate hydrates, *J. Chem. Eng. Data*, *48*, 612–616.

Ostergaard, K. K., R. Masoudi, B. Tohidi, A. Danesh, and A. C. Todd (2005), A general correlation for predicting the suppression of hydrate dissociation temperature in the presence of thermodynamic inhibitors, *J. Pet. Sci. Eng.*, *48*, 70–80.

Pearson, C., J. Murphy, and R. Hermes (1986), Acoustic and resistivity measurements on rock samples containing tetrahydrofuran hydrates—Laboratory analogs to natural-gas hydrate deposits, *J. Geophys. Res.*, *91*, 14,132–14,138.

Priest, J. A., A. I. Best, and C. R. I. Clayton (2005), A laboratory investigation into the seismic velocities of methane gas hydrate-bearing sand, *J. Geophys. Res.*, *110*, BO4102, doi:10.1029/2004JB003259.

Sloan Jr., E. D. (1998), *Clathrate Hydrates of Natural Gases*, 2nd ed., CRC Press, Boca Raton, Fla.

Uchida, T., T. Ebinuma, S. Takeya, J. Nagao, and H. Narita (2002), Effects of pore sizes on dissociation temperatures and pressures of methane, carbon dioxide, and propane hydrates in porous media, *J. Phys. Chem. B*, *106*, 820–826.

Ulrich, T. J., and T. W. Darling (2001), Observation of anomalous elastic behavior in rock at low temperatures, *Geophys. Res. Lett.*, *28*, 2293–2296.

Ulrich, T. J., K. R. McCall, and R. A. Guyer (2002), Determination of elastic moduli of rock samples using resonant ultrasound spectroscopy, *J. Acoust. Soc. Am.*, *111*, 1667–1674.

Visscher, W. M., A. Migliori, T. M. Bell, and R. A. Reinert (1991), On the normal-modes of free-vibration of inhomogeneous and anisotropic elastic objects, *J. Acoust. Soc. Am.*, *90*, 2154–2162.

Vysniauskas, A., and P. R. Bishnoi (1983), A kinetic-study of methane hydrate formation, *Chem. Eng. Sci.*, *38*, 1061–1072.

Waite, W. F., W. J. Winters, and D. H. Mason (2004), Methane hydrate formation in partially water-saturated Ottawa Sand, *Am. Mineral.*, *89*, 1202–1207.

Wilder, J. W., K. Seshadri, and D. H. Smith (2001), Modeling hydrate formation in media with broad pore size distributions, *Langmuir*, *17*, 6729–6735.

Winters, W. J., J. S. Booth, R. R. Nielsen, W. P. Dillon, and R. F. Commeau (1994), A computer-controlled gas hydrate sediment formation and triaxial test system, *Ann. N. Y. Acad. Sci.*, *715*, 490–491.

Winters, W. J., I. A. Pecher, W. F. Waite, and D. H. Mason (2004), Physical properties and rock physics models of sediment containing natural and laboratory-formed methane gas hydrate, *Am. Mineral.*, *89*, 1221–1227.

Zadler, B. J., J. H. L. Le Rousseau, J. A. Scales, and M. L. Smith (2004), Resonant ultrasound spectroscopy: Theory and application, *Geophys. J. Int.*, *156*, 154–169.

Zatsepina, O. Y., and B. A. Buffett (2001), Experimental study of the stability of CO_2-hydrate in a porous medium, *Fluid Phase Equilib.*, *192*, 85–102.

Zhang, H., R. S. Sorbello, C. Hucho, J. Herro, J. R. Feller, D. E. Beck, M. Levy, D. Isaak, J. D. Carnes, and O. Anderson (1998), Radiation impedance of resonant ultrasound spectroscopy modes in fused silica, *J. Acoust. Soc. Am.*, *103*, 2385–2394.

Zhang, W., J. W. Wilder, and D. H. Smith (2003), Methane hydrate-ice equilibria in porous media, *J. Phys. Chem. B*, *107*, 13,084–13,089.

Zhu, T., B. P. McGrail, A. Kulkarni, M. D. White, H. Phale, S. Patil, and D. Ogbe (2005), Development of a Thermodynamic Model and Reservoir Simulator for the CH_4, CO_2, and CH_4-CO_2 Gas Hydrate System, Paper 93976 presented at AAPG/SPE Western Regional Meeting, Society of Petroleum Engineering, Irvine, California.

S. Ahmed, Applied Physics and Materials Characterization Department, Pacific Northwest National Laboratory, P. O. Box 999, Richland, WA 99352, USA.

P. F. Martin, B. P. McGrail, A. T. Owen, and H. T. Schaef, Applied Geology and Geochemistry Department, Pacific Northwest National Laboratory, P. O. Box 999, Richland, WA 99352, USA. (pete.mcgrail@pnl.gov)

T. Zhu, Petroleum Engineering Department, University of Alaska, 411 Duckering Building, Fairbanks, AK 99775, USA.